Scientific Research Publishing

Journal of Geoscience and Environment Protection, 2025, 13(11), 111-131
https://www.scirp.org/journal/gep
ISSN Online: 2327-4344
ISSN Print: 2327-4336

Research on Reservoir Characteristics of the Shanxi Formation in the Eastern Yanchuan Area and Their Geological Significance

Qiyu Gao*, Meng Wang, Tianchao Guo, Xiao Yang

Yan'an Gas Field Gas Production Plant No. 5, Shaanxi Yanchang Petroleum (Group) Company Limited, Yan'an, China
Email: *1878003711@qq.com

How to cite this paper: Gao, Q. Y., Wang, M., Guo, T. C., & Yang, X. (2025). Research on Reservoir Characteristics of the Shanxi Formation in the Eastern Yanchuan Area and Their Geological Significance. *Journal of Geoscience and Environment Protection, 13,* 111-131.
https://doi.org/10.4236/gep.2025.1311007

Received: October 4, 2025
Accepted: November 16, 2025
Published: November 19, 2025

Abstract

The sandstone reservoir of the Shanxi Formation serves as a key exploration and development target in the eastern Yanchuan gas field of the Ordos Basin, where its physical properties and pore structure directly govern the enrichment and distribution of hydrocarbons. This study systematically examines the petrological features, pore types, throat structures, and petrophysical parameters of the Shanxi Formation sandstone reservoir using core observation, thin-section identification, cast thin-section and scanning electron microscopy analyses, mercury injection porosimetry, and conventional petrophysical testing. Results indicate that the reservoir predominantly comprises fine- to medium-grained sandstones, dominated by lithic sandstones, lithic quartz sandstones, and quartz sandstones as the primary lithofacies assemblages. Detrital components are chiefly quartz and metamorphic rock fragments, with cementation primarily of the pore-filling type and common siliceous and carbonate cements. Dominant pore types include dissolution pores in volcanic lithics, residual intergranular pores, and minor intercrystalline pores and microfractures. Porosity is generally low, averaging less than 6%, with permeability ranging from 0.001 to 5.577 mD. Mercury injection experiments reveal that throat sizes are predominantly small, exhibiting poor sorting and limited connectivity, classifying the reservoir overall as an ultra-low-porosity, tight type, though locally high-quality sandstone intervals are developed. Integrated analysis highlights pronounced heterogeneity in the Shanxi Formation reservoir, wherein pore preservation and dissolution processes exert significant enhancement on reservoir quality, while microfractures play a pivotal role in hydrocarbon migration and accumulation. These findings offer valuable insights for reservoir evaluation and natural gas exploration and development in the Shanxi Formation of the eastern Yanchuan gas field.

Keywords

Shanxi Formation, Reservoir Characteristics, Pore Structure, Petrophysical Evaluation, Eastern Yanchuan Gas Field

1. Introduction

The Ordos Basin is one of China's most vital energy bases, endowed with abundant petroleum, natural gas, and coal resources. Within the eastern part of the basin, specifically the Yanchuan Gas Field, the sandstone reservoirs of the Shanxi Formation constitute a critical stratigraphic interval for natural gas exploration and development (Abdulhadi et al., 2025; Zou et al., 2010; Dang et al., n.d.; Wang et al., 2016; Xue et al., 2024; Zhang et al., 2025; Zou et al., 2015). As exploration efforts intensify, the heterogeneity of the Shanxi Formation reservoirs and its impact on gas exploration success have become increasingly prominent. Accurately evaluating reservoir characteristics, elucidating pore structures, and revealing their evolutionary patterns have emerged as core scientific challenges in the field of hydrocarbon exploration and development.

The Shanxi Formation was deposited during the Early Permian, under the influence of a paralic to shallow marine shelf depositional system, exhibiting distinct regional variations in tectonic setting, sediment supply, and depositional dynamics (Lv et al., 2025; Peng et al., 2025). Studies indicate that the formation and evolution of Shanxi Formation sandstone reservoirs are governed not only by depositional processes but also profoundly modified by diagenetic alterations, particularly the superposition of compaction, cementation, and dissolution, which exert far-reaching effects on reservoir properties and pore structures.

In recent years, with the advancement of unconventional natural gas exploration and development, the focus in the Yanchuan East Gas Field of the Ordos Basin has shifted from high-productivity intervals such as the Yanchang and Shihezi Formations to deeper ones like the Shanxi Formation. During this transition, challenges including strong reservoir tightness, poor pore connectivity, and generally low petrophysical properties have surfaced, posing key barriers to efficient natural gas development (Li et al., 2021a; Poda & Talal, 2025; Tang et al., 2025a). Therefore, systematic research on the characteristics of Shanxi Formation reservoirs holds significant theoretical and practical value.

Currently, domestic and international studies on Shanxi Formation reservoirs have accumulated substantial progress, primarily focusing on depositional facies, sandstone body distribution patterns, and macroscopic petrophysical distributions, yielding rich findings (Ashraf et al., 2021; Avseth et al., 2010). However, research on microscopic pore structure features, the relationship between cementation and pore preservation, throat distribution patterns, and heterogeneity remains insufficient (Cui et al., 2022; Li et al., 2018; Tong et al., 2022; Zhong et al., 2022). This gap is particularly evident in the Yanchuan East area, where reservoir complexity and strong heterogeneity have led to relatively weak systematic petrological and pore structure investigations, thereby constraining the refinement of reservoir evaluation and the efficiency of development to some extent.

Accordingly, this study utilizes core samples, thin sections, scanning electron microscopy (SEM), and mercury injection capillary pressure (MICP) data from coring wells in the Yanchuan East area to systematically investigate the petrological characteristics, pore types, throat structures, and petrophysical properties of Shanxi Formation reservoirs. Key aspects include exploring the primary petrological features and compositional controls on reservoir properties; analyzing the influence of pore types and their development on effective reservoir formation; revealing fundamental throat structure patterns and differences between the Shan 1 and Shan 2 members; and further examining the primary factors governing the formation and preservation of high-quality reservoirs amid overall tightness. Through these investigations, this paper aims to elucidate the basic characteristics and genetic mechanisms of Shanxi Formation reservoirs from petrological, pore structural, and petrophysical perspectives, providing scientific support for natural gas exploration and development in the Yanchuan East Gas Field, while offering references for studies and practices on tight sandstone reservoirs in analogous basins across China.

2. Geological Setting

The Ordos Basin, situated in the western North China Craton, represents a major cratonic sedimentary basin in China (Ritts et al., 2009; Tian et al., 2021; Zhou et al., 2017). The basin's overall structural configuration features a north-high south-low and west-gentle east-steep pattern, with complete stratigraphic development from Archean to Cenozoic. The study area, the Yanchuan East Gas Field, lies along the eastern margin of the Ordos Basin and tectonically occupies the central Yishaan Slope, forming a vital component of the basin's eastern gas plays.

The Shanxi Formation was deposited in the Early Permian (approximately 299 Ma), stratigraphically overlying the Taiyuan Formation and underlying the Shihezi Formation (Tian et al., 2021). During this period, the basin was characterized by a paralic depositional environment, with diverse facies including delta plains, delta fronts, and shallow marine shelves. Influenced by sediment supply and paleotopography, sandstone bodies in the study area's Shanxi Formation are widely distributed, with reservoir thicknesses varying significantly, typically ranging from 10 to 40 m.

In terms of provenance, sediments of the Shanxi Formation were primarily derived from uplifts in the north and northwest, ensuring ample detrital supply with high quartz content, alongside notable proportions of volcanic and metamorphic lithics (Li et al., 2023; Tang et al., 2025b; Yan et al., 2010). Strong depositional energy imparted moderate to good sorting to the sand bodies overall, though locally rapid deposition and early compaction resulted in poorer reservoir properties.

Tectonically, the Ordos Basin during the Permian was a stable cratonic basin undergoing slow subsidence with minimal structural activity, making depositional processes the dominant control on Shanxi Formation reservoir formation (Cui et al., 2025; Li et al., 2021b; Liu et al., 2024; Yang et al., 2005). Nevertheless, subsequent diagenetic processes, especially compaction and cementation, profoundly altered sandstone porosity, establishing a background of reservoir tightening. Dissolution, to some extent, ameliorated these conditions, facilitating the development of effective reservoirs.

In summary, Shanxi Formation reservoirs formed in a paralic setting with extensive sandstone body distribution and diverse lithofacies assemblages. However, intense diagenesis has rendered them characteristically ultra-low porosity and tight, with relatively high-quality reservoir segments developed only locally.

This study is based on conventional core samples from 25 coring wells in the eastern Yanchuan Gas Field, spanning the Shanxi Formation at depths of 2182 - 2831 m (Shan 1 Member: −2460 - 2697 m; Shan 2 Member: −2487 - 2819 m). A total of 65 core plugs were analyzed for petrophysical properties (porosity and permeability, both *in-situ* and overburden-corrected), with over 1200 samples contributing to statistical distributions (Section 5.1). Thin-section analysis (cast thin-sections under plane-polarized and cross-polarized light) was performed on 65 samples (45 from Shan 1, 20 from Shan 2) to quantify detrital components, cements, and areal porosity/pore types. Scanning electron microscopy (SEM) observations, including backscattered electron imaging, were conducted on selected subsamples (−20 from key intervals) to characterize clay minerals, cements, and micropores at resolutions of 0.1 - 1 μm. High-pressure mercury injection capillary pressure (MICP) experiments followed SY/T 5810-2013 standards, using 77 samples (29 from Shan 1, 48 from Shan 2) on a Micromeritics AutoPore IV porosimeter (maximum pressure −400 MPa) to derive throat size distributions, sorting parameters, and connectivity metrics. All analyses were conducted at the Key Laboratory of Petroleum Resources, Research Institute of Petroleum Exploration and Development.

3. Reservoir Petrology

Based on core and thin-section observations from coring wells, the lithology of Shanxi Formation reservoirs is dominated by fine-grained sandstones, primarily light gray fine-grained sandstones, followed by light gray medium-grained sandstones and gray muddy siltstones. In the Shan 1 Member, grain sizes predominantly range from 0.4 to 0.7 mm, with medium- to coarse-grained textures prevailing; sorting is moderate to good, with minor poorly sorted intervals; roundness is chiefly subangular, followed by subrounded, rounded, and angular; grain contacts are mainly convex-concave and point-line, with lesser point, line, and line-convex-concave contacts; cementation is primarily pore-filling, secondary contact type. In the Shan 2 Member, grain sizes range from 0.2 to 1.1 mm, with medium- to coarse-grained dominance; sorting is moderate to good, with minor poor sorting; roundness is mainly subangular, followed by subrounded, rounded, and angular; grain contacts are chiefly convex-concave and line, with minor point, point-line, and line-convex-concave; cementation is pore-filling dominant. Details are elaborated below.

3.1. Detrital Components and Contents

Detrital components in Shanxi Formation sandstones are dominated by quartz, followed by various lithics, clay minerals, mica, and minor heavy minerals (Table 1) (Li et al., 2021b; Xu et al., 2021a). Specifically, in the Shan 1 Member, quartz content ranges from 29.7% to 96.7% (average 67.1%); lithic content from 13.3% to 68.9% (average 31.6%), dominated by metamorphic lithics (2.3% - 55.4%, average 22.9%), followed by igneous lithics (0.5% - 12.5%, average 3.5%), and minor sedimentary lithics (0.3% - 10.2%, average 1.6%). In the Shan 2 Member, quartz content ranges from 47.89% to 94.32% (average 71.77%); lithic content from 5.68% to 52.11% (average 28.14%), dominated by metamorphic lithics (0% - 44.58%, average 13.06%), followed by igneous lithics (0% - 39.43%, average 11.85%), and minor sedimentary lithics (0% - 8.14%, average 0.83%). According to the Chinese National Standard for Sedimentary Rock Classification and Nomenclature (GB/T 17412.2-1998), sandstones in the Shan 1 Member of the study area are primarily lithic sandstones, lithic quartz sandstones, and quartz sandstones; those in the Shan 2 Member are similarly dominated by lithic sandstones, lithic quartz sandstones, and quartz sandstones (Figures 1-2).

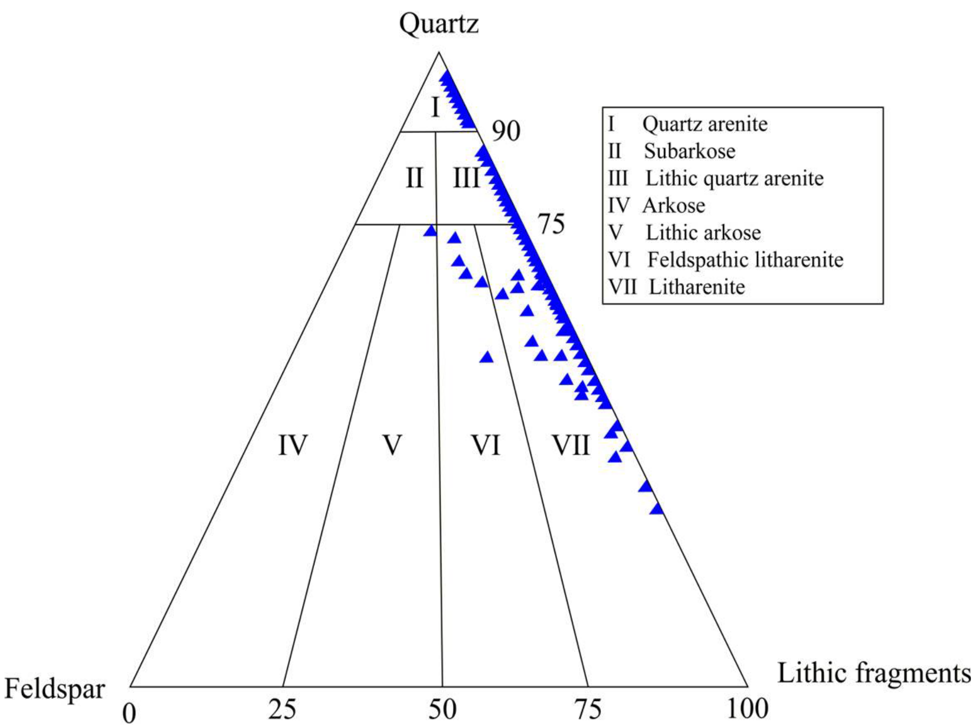

Figure 1. Triangular classification diagram for sandstones of the Shan 1 Member in the Yanchuan East area.

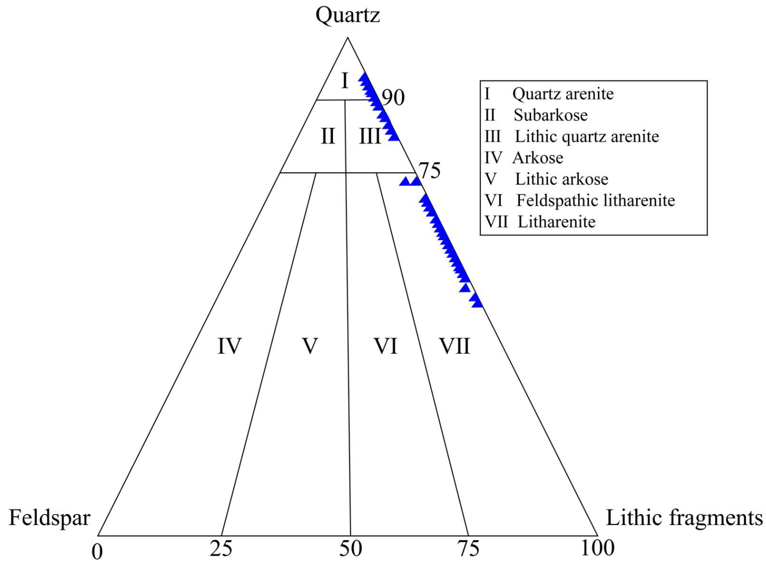

Figure 2. Triangular classification diagram for sandstones of the Shan 2 Member in the Yanchuan East area.

Table 1. Detrital component contents (%) in Shanxi Formation reservoir rocks, Yanchuan East area.

Member	No. of Samples	Quartz	Feldspar	Lithics	Intergranular Fill Components						
					Calcite	Dolomite	Ferroan Dolomite	Siderite	Clay Minerals	Anhydrite	Other
Shan 1	45	67.11	1.27	31.62	1.81	0.40	4.18	0.98	1.95	1.15	1.13
Shan 2	20	71.77	0.01	28.14	2.96	2.04	2.23	0.47	1.94	1.04	1.42

3.2. Interstitial Component Characteristics

In the Yanchuan East area, interstitial components in Shanxi Formation reservoirs are dominated by clay minerals, including biotite (0% - 7%, average 2.23%), kaolinite (0% - 10%, average 1.27%), and chlorite (0% - 6%, average 1.04%). Secondary components comprise siliceous and carbonate cements (**Table 2**), with siderite being the most abundant (0% - 28%, average 2.96%), followed by silica (0% - 6%, average 1.94%) and kaolinite (0% - 10%, average 1.27%); chlorite contents are relatively low (0% - 6%, average 1.04%) (**Figures 3-5**).

Table 2. Cement compositions (%) in Shanxi Formation reservoir sandstones, Yanchuan East area, Yanchuan Gas Field.

Member	Kaolinite	Biotite	Chlorite	Tuffaceous Material	Siderite	Ferroan Dolomite	Silica
Shan 1	0.49	4.18	1.15	0.56	1.81	0.40	1.95
Shan 2	1.27	2.23	1.04	0.15	2.96	2.04	1.94

Cement contents differ between the Shan 1 and Shan 2 members, with the Shan 2 Member exhibiting higher biotite and siderite, followed by silica, kaolinite, ferroan dolomite, and chlorite, along with minor tuffaceous material; in the Shan 1 Member, chlorite and kaolinite are more abundant, followed by silica and biotite (**Table 2**; **Figures 3-4**).

Siliceous cement is ubiquitous in the main gas-bearing intervals of the study area (Figures 3-4), with contents ranging from 1.03% to 2.40%. It occurs in diverse forms, such as pore-filling and syntaxial overgrowths. Due to its resistance to dissolution, siliceous cement significantly impairs reservoir quality by hindering secondary pore development. Carbonate cements primarily include siderite, ferroan dolomite, and minor siderite (Figures 3-4, Figure 6), with contents ranging from 0.4% to 6.79%; siderite and ferroan dolomite are relatively enriched in the Shan 2 Member.

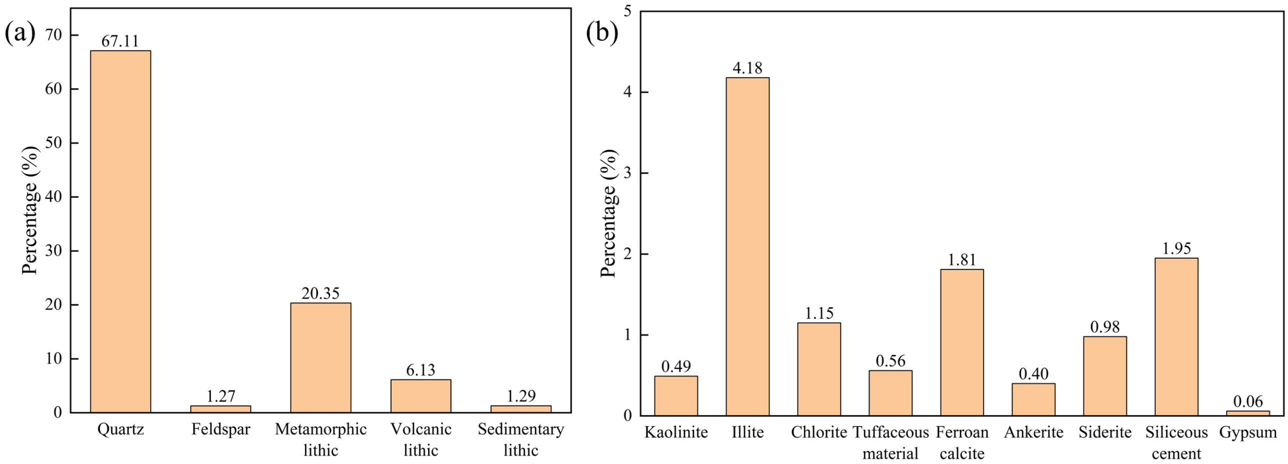

Figure 3. Bar chart of average detrital (a) and interstitial component (b) contents in the Shan 1 Member, Yanchuan East area.

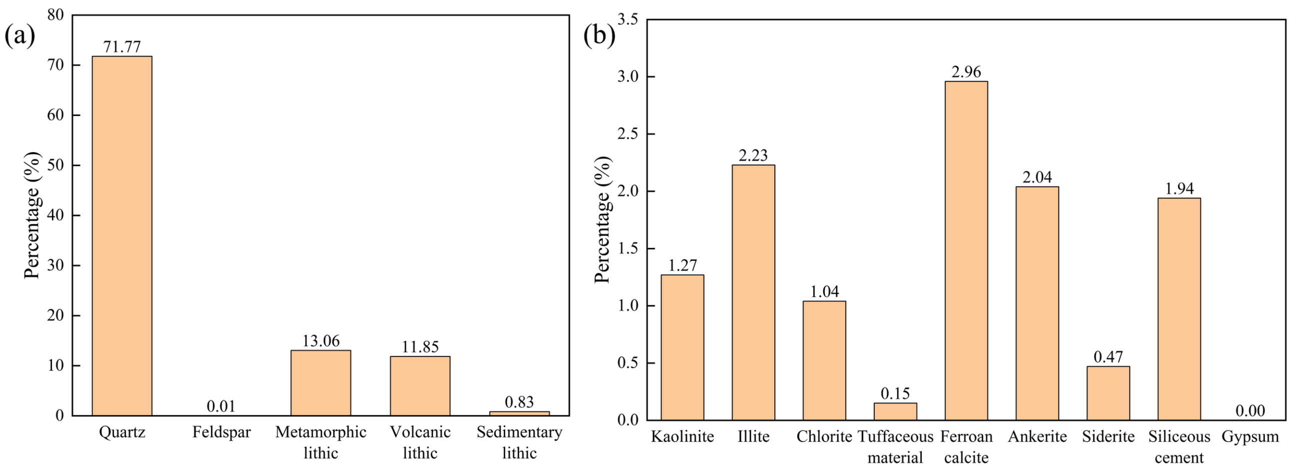

Figure 4. Bar chart of average detrital (a) and interstitial component (b) contents in the Shan 2 Member, Yanchuan East area.

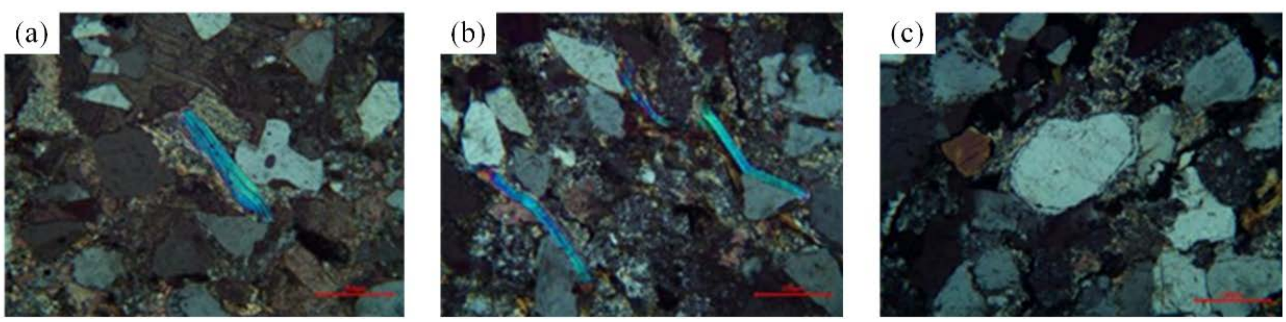

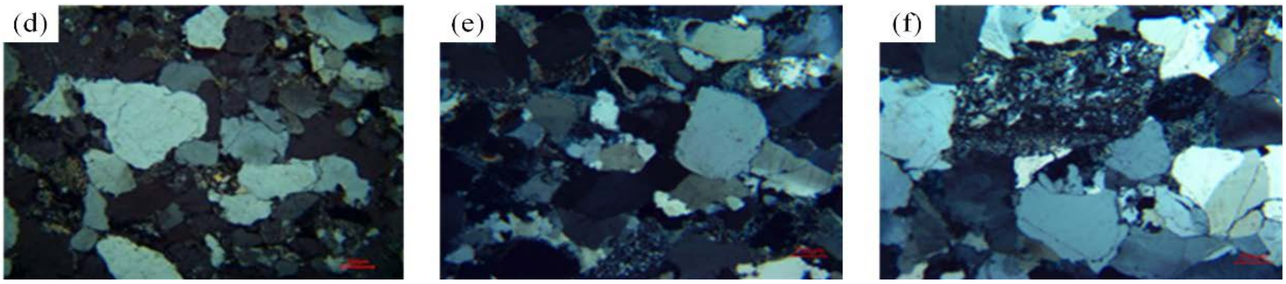

(a) Well Yan 2065, Shanxi Formation, 2261.08 - 2261.28 m, fine-grained lithic quartz sandstone, deformed mica clasts, early calcite cement. (b) Well Yan 2065, Shanxi Formation, fine-grained lithicraph quartz sandstone, deformed mica clasts, early calcite cement. (c) Well Yan 2065, Shanxi Formation, medium-grained lithic quartz sandstone, 2264.97 - 2265.18 m, widespread secondary quartz overgrowths. (d) Well Yan 2065, Shanxi Formation, medium-grained lithic quartz sandstone, 2269.06 - 2269.27 m, secondary quartz overgrowths with minor calcite. (e) Well Yan 343, Shan 1 Member, 2460.02 - 2460.15 m, lithic quartz sandstone, intense compaction, high metamorphic lithic content, strongly deformed volcanic lithics. (f) Well Yan 343, Shan 1 Member, 2461.42 - 2461.56 m, coarse-grained lithic quartz sandstone, secondary quartz overgrowths, kaolinitization and illitization of lithics.

Figure 5. Petrographic features of Shanxi Formation detrital sandstones under plane-polarized light.

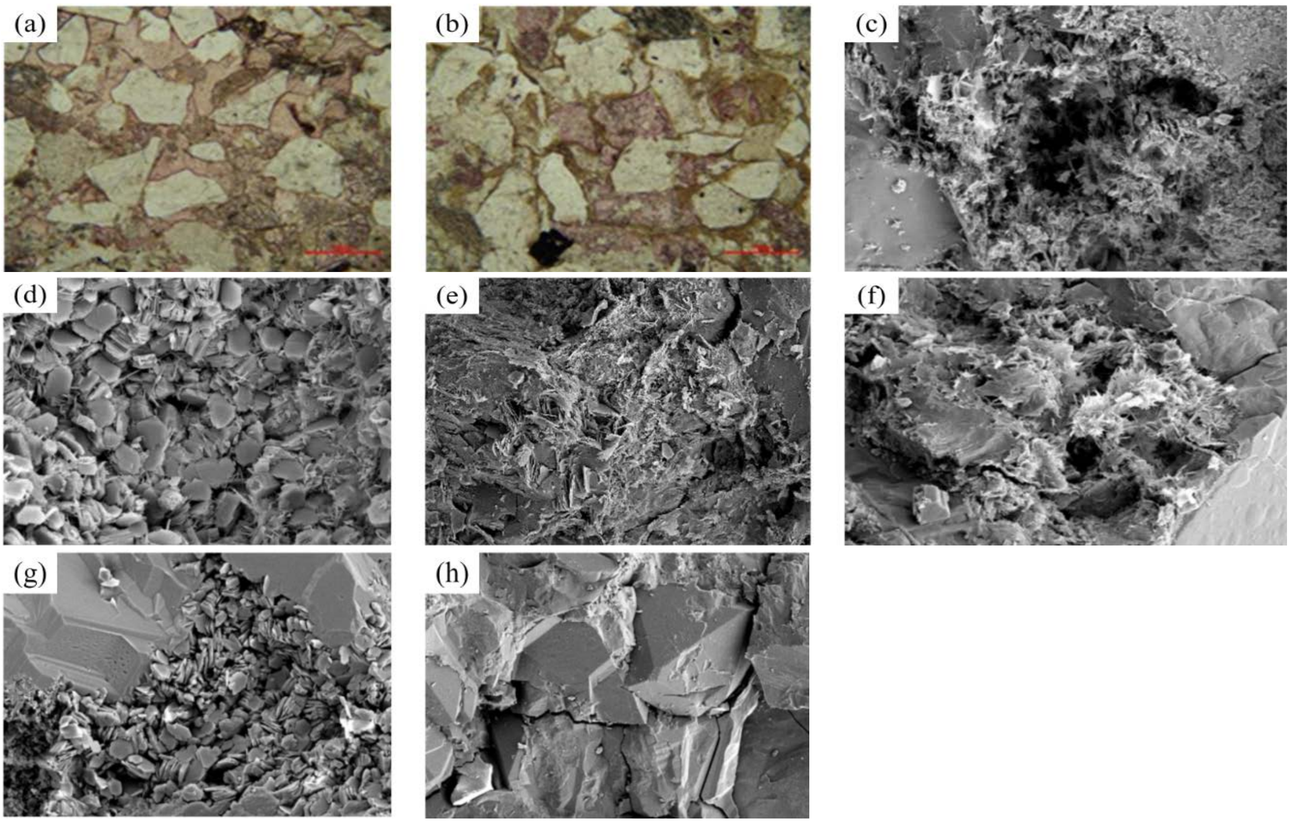

(a) Well Yan 2065, Shanxi Formation, 2261.08 - 2261.28 m, fine-grained lithic quartz sandstone, basal calcite cement with chlorite coatings. (b) Well Yan 2065, Shanxi Formation, 2261.42 - 2261.54 m, fine-grained lithic quartz sandstone, calcite filling dissolution pores with minor chlorite. (c) Well Yan 343, 2460.98 - 2461.12 m, Shan 1 Member, light gray medium sandstone, filamentous illite, platy chlorite, kaolinite, and intergranular pores. (d) Well Yan 343, 2462.52 - 2462.62 m, Shan 1 Member, light gray gas-bearing coarse sandstone, kaolinite filling intergranular pores. (e) Well Yan 147, 2386.80 - 2386.94 m, Shan 1 Member, gray-white gas-bearing gravelly medium sandstone. (f) Well Yan 311, 2697.19 - 2697.29 m, Shan 1 Member, intergranular filamentous illite, minor platy chlorite, and kaolinite. (g) Well Yan 349, 2829.49 - 2831.28 m, Shan 1 Member, quartz overgrowths and intergranular kaolinite clay fills. h. Well Yan 328, 2450.98 - 2451.17 m, Shan 1 Member, intense quartz overgrowths, intergranular calcite cement, and residual intergranular fissures.

Figure 6. Scanning electron microscopy features of cements in Shanxi Formation detrital sandstones.

4. Reservoir Pore Types and Throat Structure Characteristics

4.1. Pore Types in the Shanxi Formation

The Shanxi Formation in the Yanchuan East area primarily features three pore types: residual intergranular pores, secondary dissolution pores, and intercrystalline pores (Gao et al., 2019; Zhang et al., 2022). Secondary dissolution pores mainly include feldspar and volcanic lithic dissolution pores.

4.1.1. Residual Intergranular Pores

Shan 1 Member reservoir sandstones have undergone intense mechanical compaction, resulting in widespread residual intergranular pores between rigid grains such as quartz and minor feldspar, albeit in low proportions (Shan et al., 2021; Xiao et al., 2023; Xu et al., 2021b). These pores are commonly coated by chlorite clay rims or partially filled by illite, kaolinite, muddy matrix, or secondary quartz overgrowths (**Figure 7(a)-(b)**; **Figure 8(a)-(c)**). They exhibit irregular shapes with throat diameters typically 10 - 30 μm. Residual intergranular pores are more developed in sandstones with high quartz content; higher volcanic lithic contents lead to plastic deformation under compaction, sharply reducing or eliminating these pores.

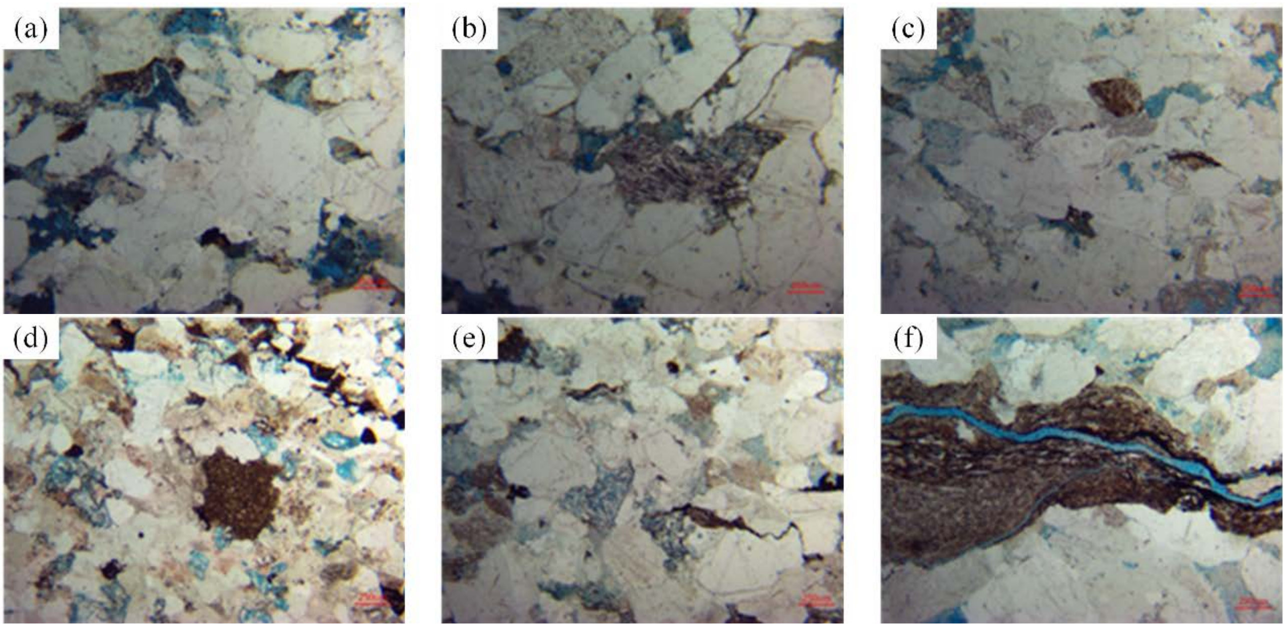

(a) Well Yan 343, Shan 1, 2460.02 – 2460.15 m, volcanic lithic dissolution pores, areal porosity 8%. (b) Well Yan 343, Shan 1, 2460.83 - 2460.98 m, minor intergranular and volcanic lithic dissolution pores, areal porosity 3%. (c) Well Yan 155, Shan 1, 2536.20 - 2536.31 m, volcanic lithic dissolution pores and minor intergranular pores, areal porosity 6%. (d) Well Yan 155, Shan 1, 2537.89 - 2537.98 m, volcanic lithic dissolution pores and minor intergranular pores, areal porosity 8%. (e) Well Yan 126, Shan 1, 2672.79 - 2672.90 m, volcanic lithic dissolution pores and minor intergranular pores, areal porosity 5%. (f) Well Yan 343, Shan 1, 2462.20 - 2462.32 m, minor microfractures, areal porosity 1%.

Figure 7. Cast thin-section pore types and development features in Shan 1 Member sandstones, Yanchuan East area.

4.1.2. Secondary Dissolution Pores

These primarily include intragranular dissolution pores in lithics and feldspar, dominated by lithic dissolution pores with minor feldspar ones. Intragranular pores occur as isolated or honeycomb forms, with dissolution along cleavage planes (Figure 7(c)-(e); Figure 8(d)-(g)). Minor intergranular dissolution pores exhibit irregular, bay-like shapes with uneven sizes and distributions. Throat diameters typically range from 20 to 70 μm, averaging −30 μm (Figure 9).

4.1.3. Microfractures

Microfractures are locally developed in the study area. Core observations reveal multiple high-angle fractures in gas-bearing intervals across several wells. Cast thin sections confirm their presence. These fractures enhance pore connectivity in reservoir sandstones and serve as conduits for hydrocarbon migration. Overall, fracture density in the Shanxi Formation is low (Figure 7(f)).

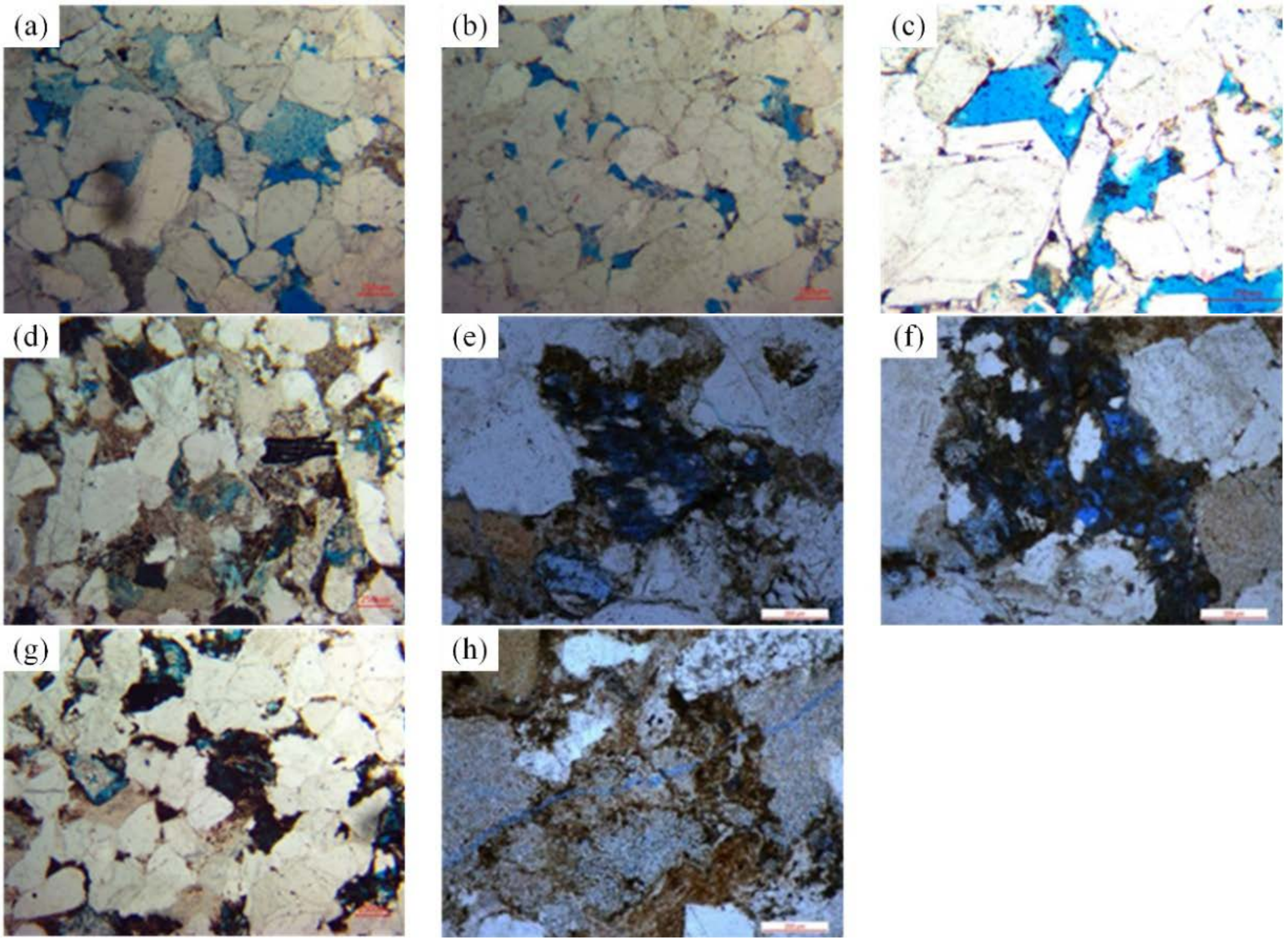

(a) Well Yan 250, Shan 2, 2755.77 - 2755.88 m, intergranular and lithic dissolution pores, areal porosity 7%. (b) Well Yan 338, Shan 2, 2668.09 - 2668.23 m, intergranular pores and minor feldspar/lithic dissolution pores, areal porosity 5.0%. (c) Well Yan 165, Shan 2, 2613.09 - 2613.17 m, intergranular pores, areal porosity 5.7%. (d) Well Yan 347, Shan 2, 2816.19 - 2816.38 m, minor lithic dissolution pores, areal porosity 3%. (e) Well Yan 347, Shan 2, 2817.11 - 2817.25 m, volcanic lithic dissolution pores, areal porosity 5.1%. (f) Well Yan 333, Shan 2, 2755.77 - 2755.88 m, lithic dissolution pores and minor intergranular pores, areal porosity 5%. (g) Well Yan 336, Shan 2, 2487.37 - 2487.49 m, minor intergranular, volcanic lithic, and feldspar dissolution pores, areal porosity 2%. (h) Well Yan 347, Shan 2, 2819.25 - 2819.45 m, minor microfractures, areal porosity 1%.

Figure 8. Cast thin-section pore types and development features in Shan 2 Member sandstones, Yanchuan East area.

4.1.4. Intercrystalline Pores

Intercrystalline pores vary in size and distribution, generally small, influenced by crystal size and packing density. They primarily occur within authigenic clay mineral clusters such as kaolinite, chlorite, and illite. Pore diameters are minute, typically < 0.01 mm (Figure 9).

Statistical results indicate that areal porosity in the Shan 2 Member ranges from 1.3% to 5.6% (average 3.55%), dominated by volcanic lithic dissolution pores (0.5% – 5.0%, average 2.78%) and residual intergranular pores (0.5% – 6.3%, average 0.75%), with minor microfractures and intercrystalline micropores (average −0.3%). In the Shan 1 Member, areal porosity ranges from 1.5% to 6.5% (average 3.80%), dominated by volcanic lithic dissolution pores (0.3% – 5.2%, average 2.95%) and intergranular pores (0.5% – 5.4%, average 0.85%), with microfractures and intercrystalline pores averaging −0.35% (Table 3).

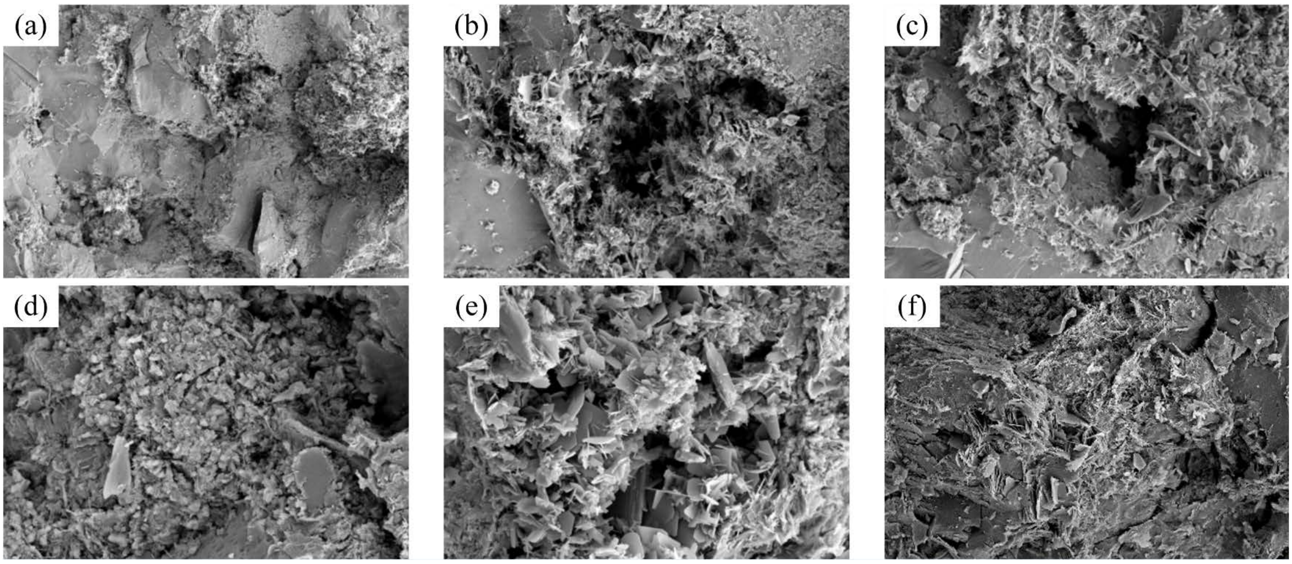

(a) Well Yan 343, 2460.98 - 2461.12 m, Shan 1 Member, minor residual intergranular pores. (b) Well Yan 343, 2460.98 - 2461.12 m, Shan 1 Member, intragranular feldspar dissolution pores partially filled by clay minerals. (c) Well Yan 179, 2182.26 - 2182.40 m, Shan 1 Member, clay fills and residual intergranular pores. (d) Well Yan 343, 2462.52 - 2462.62 m, Shan 1 Member, volcanic lithic dissolution pores and kaolinite cements. (e) Well Yan 179, 2182.26 - 2182.40 m, Shan 1 Member, intercrystalline micropores in clay minerals and intergranular pores. (f) Well Yan 147, 2386.80 - 2386.94 m, Shan 1 Member, residual intergranular pores and intercrystalline micropores.

Figure 9. Scanning electron microscopy pore types and development features in Shan 1 Member sandstones, Yanchuan East area.

Table 3. Pore type statistics (%), Yanchuan east area, Shanxi formation, Yanchuan gas field.

Member	Residual Intergranular Pores (%)	Feldspar Dissolution Pores (%)	Lithic Dissolution Pores (%)	Intercrystalline Pores (%)	Matrix Dissolution Pores (%)	Microfractures (%)	Areal Porosity (%)
Shan 1	0.85	0.15	2.95	0.10	0.00	0.10	3.80
Shan 2	0.75	0.12	2.78	0.15	0.00	0.15	3.55

4.2. Throat Structure Characteristics

High-pressure mercury intrusion (HPMI) porosimetry evaluates pore structure using parameters categorized as follows: throat size (displacement pressure and maximum throat radius, median pressure and median radius, average throat volume ratio); distribution characteristics (sorting coefficient, skewness, kurtosis); and connectivity (maximum mercury saturation and withdrawal efficiency) (Fu et al., 2021; Xu et al., 2019; Zhang et al., 2020).

The statistical parameters describing pore-throat distribution were calculated following the standard definitions in SY/T 6285-2011. The sorting coefficient (So), skewness coefficient (Sk), and kurtosis (Ku) were derived from the cumulative frequency curve of throat radius on a logarithmic scale using the following formulas (after Xu et al., 2019):

$$S_o = \sqrt{\frac{R_{84}/R_{16}}{R_{50}^2}} \tag{1}$$

$$S_k = \frac{\left(R_{84} + R_{16} - 2R_{50}\right)}{R_{84} - R_{16}} \tag{2}$$

$$K_u = \frac{R_{97.5} - R_{2.5}}{2.44\left(R_{84} - R_{16}\right)} \tag{3}$$

where R_x represents the throat radius corresponding to x% mercury saturation. These coefficients respectively characterize the uniformity, symmetry, and sharpness of the pore–throat size distribution. Analysis of HPMI parameters from sandstone samples in the study area (**Table 4**) reveals the following throat structure characteristics in Shanxi Formation sandstones:

Table 4. High-pressure mercury intrusion parameter statistics for Shanxi Formation sandstones, Yanchuan East area, Yanchuan Gas Field.

Parameter			Physical Properties		Pore-Throat Size			Pore-Throat Sorting Characteristics			Pore-Throat Connectivity	
Formation	Number of Samples		Porosity (%)	Permeability (mD)	Displacement Pressure (MPa)	Median Pressure (MPa)	Median Radius (μm)	Pore-Throat Sorting Coefficient	Coefficient of Variation	Skewness Coefficient	Maximum Mercury Saturation (%)	Withdrawal Efficiency (%)
Shan 1	29	Minimum	1.79	0.012	0.01	1.77	0.01	0.02	0.15	−2.08	44.66	13.38
		Maximum	11.57	0.747	4.10	88.72	0.90	5.10	1.87	1.93	99.04	49.98
		Average	4.02	0.111	1.15	30.51	0.13	2.47	0.83	1.00	72.79	38.04
Shan 2	48	Minimum	1.80	0.001	0.01	4.66	0.01	1.38	0.11	−1.44	36.42	8.26
		Maximum	9.10	3.795	3.57	70.32	0.16	4.22	0.24	2.49	94.50	45.51
		Average	6.51	0.764	0.63	40.01	0.05	2.19	0.16	1.30	70.72	21.81

In the Shan 1 Member sandstones, displacement pressure ranges from 0.01 to 4.10 MPa (average 1.15 MPa); median pressure spans 1.77 to 88.72 MPa (average 30.51 MPa); median radius ranges from 0.01 to 0.90 μm (average 0.13 μm), indicating strong throat heterogeneity. Sorting coefficients range from 0.02 to 5.10 (average 2.47), reflecting poor sorting; skewness ranges from 0.15 to 1.87 (average 0.83). Maximum mercury saturation varies from 44.66% to 99.04% (average 72.79%), signifying limited connectivity. Overall, Shan 1 Member throats are small, poorly sorted, and poorly connected.

In the Shan 2 Member sandstones, displacement pressure ranges from 0.01 to 3.57 MPa (average 0.63 MPa); median pressure spans 4.66 to 70.32 MPa (average 40.01 MPa); median radius ranges from 0.01 to 0.16 μm (average 0.05 μm), indicating predominantly small throats. Sorting coefficients range from 1.38 to 4.22 (average 2.19), moderate sorting; skewness ranges from 0.11 to 0.24 (average 0.16), better sorted than Shan 1. Maximum mercury saturation varies from 36.42% to 94.50% (average 70.72%). Overall, Shan 2 Member throats are small, moderately sorted, and moderately connected.

Referencing the classification standards for clastic reservoir pore structures in the Evaluation Method for Oil and Gas Reservoirs (SY/T 6285-2011), which delineates types based on displacement pressure (<0.7 MPa for low; 0.7 – 2.0 MPa for moderate; >2.0 MPa for high), median throat radius (>1 μm for fine; 0.1 – 1 μm for microfine), skewness (>0 coarse-skewed; <0 fine-skewed), and curve morphology (plateau vs. steep slopes), analysis of HPMI parameters, combined with petrophysical properties and capillary pressure curve shapes, delineates four pore structure types in the Upper Paleozoic sandstones of the Yanchuan East and Yuanlongsi blocks (**Table 4**; **Figure 10**).

Type I (Low Displacement Pressure—Relatively Fine-Throated):

Curves exhibit displacement pressure of 0.01 - 1.74 MPa (average 0.52 MPa), median pressure of 0.33 - 21.21 MPa (average 3.08 MPa), median throat radius of 0.09 - 11.26 μm (average 1.73 μm), skewness of –0.22 to 2.49 (average 0.94, coarse-skewed), kurtosis of 0.14 - 0.33 (average 0.18), and maximum mercury saturation of 83.65% – 99.04% (average 92.22%). Capillary pressure curves trend toward the lower left with broad horizontal plateaus (**Figure 10(a)**). These represent relatively fine-throated reservoirs with variable pore sorting. Corresponding porosities range from 2.10% to 9.00% (average 6.33%), permeabilities from 0.057 to 4.723 mD (geometric mean 0.836 mD). Common in quartz sandstones with composite residual intergranular pores enhanced by intense dissolution, featuring coexisting large and small pores, coarse throats, and good connectivity—high-quality reservoirs.

Type II (Moderate Displacement Pressure—Fine-Throated):

Curves show displacement pressure of 0.01 - 6.32 MPa (average 0.60 MPa), median pressure of 0.27 - 36.15 MPa (average 4.66 MPa), median throat radius of 0.02 - 6.66 μm (average 1.29 μm), skewness of –0.28 to 2.11 (predominantly coarse-skewed), kurtosis of 0.11 - 1.04 (average 0.30), and maximum mercury saturation of 72.90% - 95.80% (average 83.29%). Curves slightly shift left-downward, with or without broad plateaus (**Figure 10(b)**). These fine-throated reservoirs have variable sorting. Porosities range from 1.82% to 11.57% (average 6.27%), permeabilities from 0.016 to 4.143 mD (geometric mean 0.688 mD). Prevalent in quartz, lithic quartz, or lithic sandstones with intergranular dissolution, lithic dissolution, or intercrystalline pores from intense dissolution and authigenic kaolinite, moderate connectivity—good reservoirs. Statistics show highest prevalence in Shan 1.

Type III (Moderate Displacement Pressure—Microfine-Throated):

Table 5. Pore structure type classification statistics (%) for sandstone samples, Yanchuan East area, Yanchuan Gas Field.

Formation	Pore Structure Type			
	I	II	III	IV
Shan 1	16.67%	38.89%	33.33%	11.11%
Shan 2	10.42%	16.67%	45.83%	27.08%

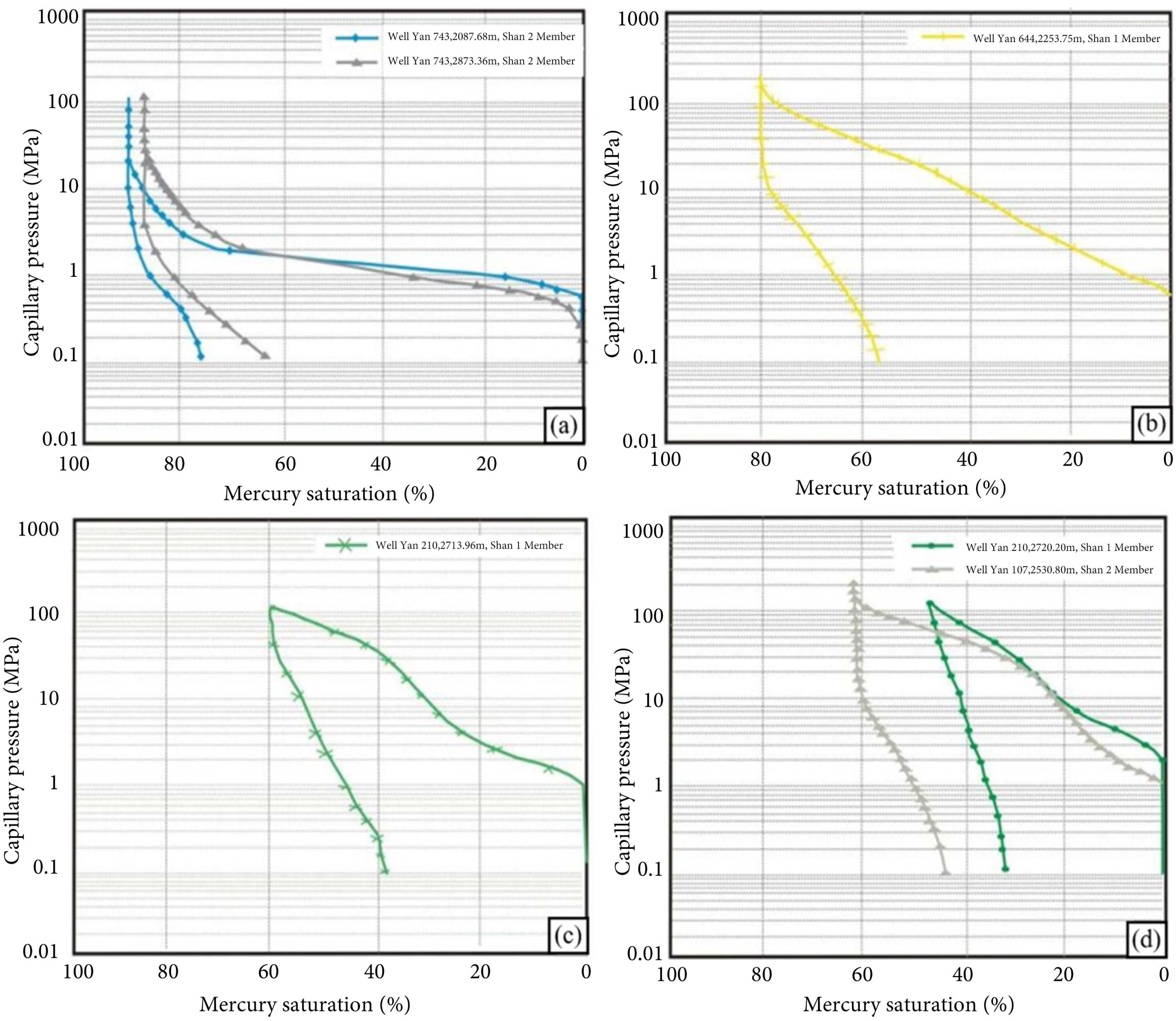

Figure 10. Representative capillary pressure curves for Shanxi Formation reservoir sandstones, Yanchuan East area.

Curves exhibit displacement pressure of 0.02 – 1.82 MPa (average 0.70 MPa), median pressure of 3.26 – 88.72 MPa (average 43.96 MPa), median throat radius of 0.14 - 0.62 μm (average 0.34 μm), skewness of 0.90 – 2.69 (fine- to coarse-skewed), kurtosis of 0.12 – 0.51 (average 0.27), and maximum mercury saturation of 63.40% - 91.26% (average 78.22%). Curves form steep, platform-less slopes (**Figure 10(c)**). Porosities range from 0.80% to 1.63% (average 1.07%), permeabilities from 0.012 to 1.681 mD (geometric mean 0.257 mD). Common in lithic quartz or lithic sandstones with intercrystalline or intragranular dissolution pores, small pores, moderate sorting and connectivity.

Type IV (High Displacement Pressure—Microfine-Throated):

Curves show displacement pressure of 0.13 - 7.61 MPa (average 1.53 MPa), median pressure >50 MPa, median throat radius of 0.02 - 0.20 μm (average 0.13 μm), skewness of –2.08 to 2.23 (predominantly fine-skewed), kurtosis of 0.08 – 0.80 (average 0.32). Curves form convex, steep upper-right slopes (**Figure 10(d)**). Porosities range from 1.79% to 5.30% (average 3.19%), permeabilities from 0.003 to 0.131 mD (geometric mean 0.024 mD). Sandstones lack visible pores, dominated by micropores or kaolinite intercrystalline pores, small throats, poor connectivity—ineffective reservoirs. Statistics indicate higher prevalence in Shan 2.

Statistics reveal that Shan 1 is dominated by Types II and III (better reservoir quality), while Shan 2 by Types III and IV (poorer quality) (**Table 5**).

5. Diagenesis and Reservoir Evolution Analysis

5.1. Reservoir Petrophysical Characteristics

5.1.1. Overburden-Corrected Porosity-Permeability Characteristics

Statistical analysis of overburden-corrected petrophysical data from over 1200 core samples across 25 wells in the Yanchuan East area indicates: For Shan 1 Member reservoir sandstones, corrected porosity ranges from 0.8% to 12.9% (average 5.3%, median 5.4%); corrected permeability from 0.002 to 0.481 mD (geometric mean 0.040 mD, median 0.039 mD). For Shan 2 Member, corrected porosity ranges from 1.3% to 11.9% (average 5.1%, median 5.0%); corrected permeability from 0.001 to 5.577 mD (geometric mean 0.047 mD, median 0.030 mD) (**Table 6**).

Table 6. Overburden-corrected petrophysical parameter statistics for Shanxi Formation sandstone reservoirs, Yanchuan East area.

Formation	Overburden Porosity (%)				Overburden Permeability (mD)			
	Minimum	Maximum	Average	Median	Minimum	Maximum	Average	Median
Shan 1	0.8	12.9	5.3	5.4	0.002	0.481	0.040	0.039
Shan 2	1.3	11.9	5.1	5.0	0.001	5.577	0.047	0.030

5.1.2. *In-Situ* Porosity-Permeability Characteristics

1) Shan 1 Member

Statistical analysis of core petrophysical data indicates that *in-situ* porosity in the Shan 1 Member reservoirs ranges from 0.38% to 13.30% (average 4.09%, median 3.81%). The main porosity range is 2% - 8% (93.10%), with > 8% comprising 4.36% and < 2% 2.5%; permeability ranges from 0.01 to 1.6 mD (geometric mean 0.61 mD, median 0.04 mD). The main permeability range is 0.01 - 0.2 mD (92.28%), with > 0.2 mD comprising 7.72% (**Figure 11**).

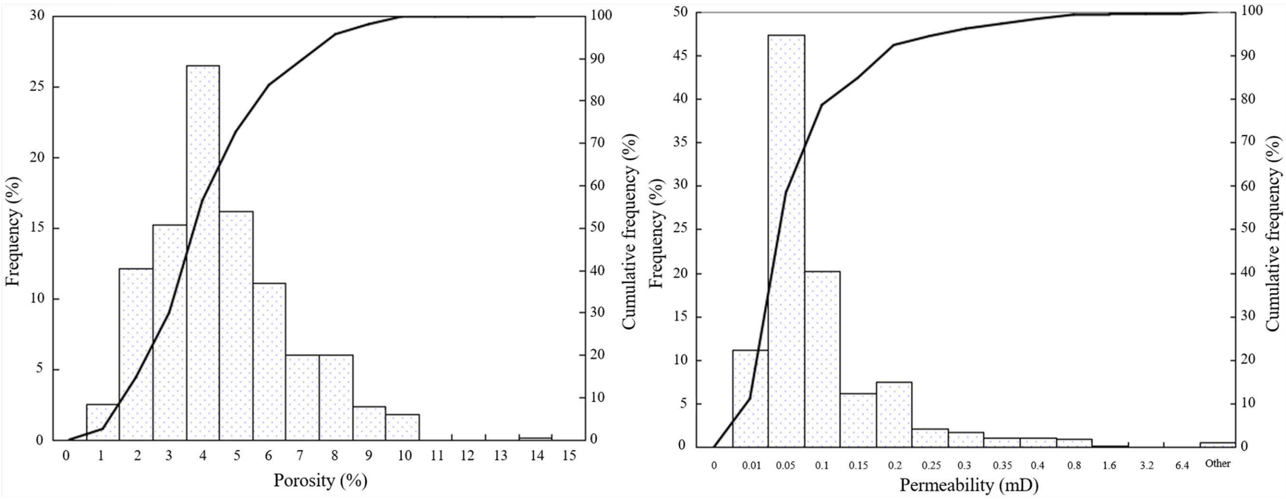

Figure 11. Histogram of *in-situ* core petrophysical distributions for Shan 1 Member, Yanchuan East area.

2) Shan 2 Member

In-situ porosity ranges from 0.38% to 13.63% (average 4.74%, median 4.33%). The main range is 2% - 8% (86.59%), with > 8% 9.60% and < 2% 3.8%; permeability ranges from 0.01 to 4.08 mD (geometric mean 0.14 mD, median 0.05 mD). The main range is 0.01 - 0.2 mD (87.78%), with > 0.2 mD 12.22% (**Figure 12**).

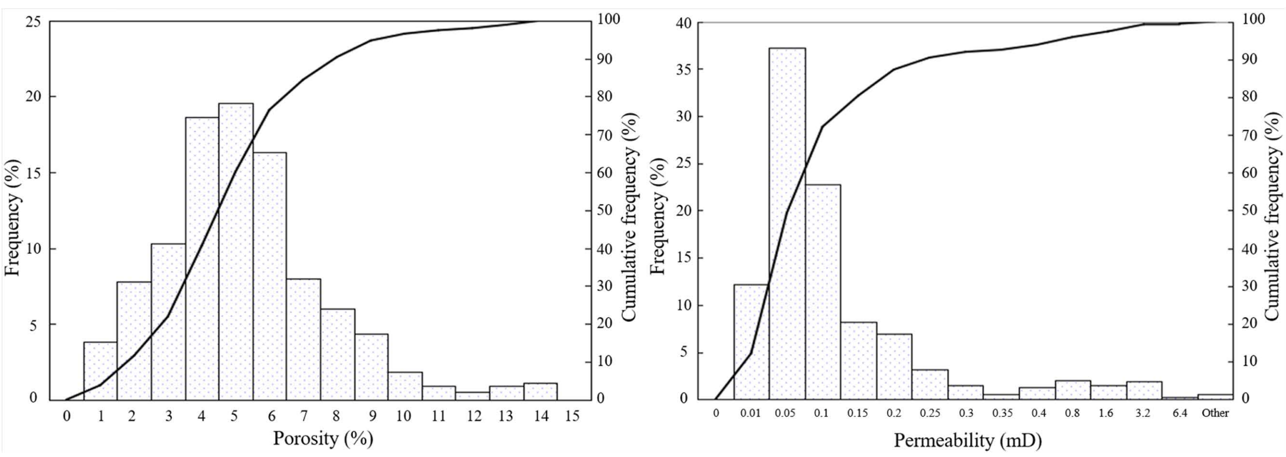

Figure 12. Histogram of *in-situ* core petrophysical distributions for Shan 2 Member, Yanchuan East area.

The observed petrophysical disparities between Shan 1 (higher average porosity 4.09% vs. 4.74% in Shan 2, but superior permeability 0.61 mD geometric mean vs. 0.14 mD; **Figures 11-12**) stem from depositional and provenance variations outlined in Section 2. Shan 1's medium- to coarse-grained dominance (0.4 - 0.7 mm) and higher metamorphic lithic input from northern uplifts (average 22.9%) reflect higher-energy delta-front facies, promoting better initial sorting and roundness that buffered early compaction (Section 3). Conversely, Shan 2's finer variability (0.2 - 1.1 mm) and elevated igneous lithics (11.85%) indicate proximal delta-plain influences with rapid deposition, exacerbating plastic deformation and siderite cementation (**Tables 1-2**), thus poorer throat connectivity (Section 4.2). This facies-provenance linkage implies that well placement should prioritize Shan 1 intervals in delta-front paleotopographic highs for optimal drainage, potentially increasing recovery by 15% - 20% over uniform targeting (cf. Li et al., 2023).

5.1.3. Diagenetic Controls on Porosity Loss

Mechanical compaction, intensified by high volcanic lithic content (up to 55.4% in Shan 1; Section 3.1), accounts for the majority of porosity reduction (−45% - 65% loss from depositional −25% - 30% to observed < 6%), as evidenced by deformed grains and convex-concave contacts (**Figures 5(e)-(f)**). In contrast, cementation contributes −15% - 25% additional loss, with siliceous cements (average 1.94%; pore-filling overgrowths) being more detrimental than carbonates (e.g., siderite at 2.96%, often ferroan and less pervasive) due to their resistance to later dissolution (Worden and Burley, 2003). For instance, SEM imaging (**Figure 6(h)**) reveals intense quartz overgrowths occluding residual intergranular pores in Shan 1 sandstones, locally reducing effective porosity by >2% compared to siderite-rimmed intervals (**Figure 6(b)**). This differential impact underscores the need for targeted dissolution enhancement in siliceous-dominated zones to mitigate tightening.

5.2. Comprehensive Reservoir Evaluation and Classification

According to the petrophysical classification standards in the Specifications for Calculation of Oil and Gas Reserves (DZ/T 0217-2020) (**Table 7**) (Fan et al., 2024; Li et al., 2024), reservoirs are divided into six classes. Core analysis in the Yanchuan East block of the Yanchuan Gas Field shows: For effective Shan 2 reservoirs, corrected porosity ranges from 3.0% to 11.9% (average 5.4%, median 5.2%); corrected permeability from 0.010 to 5.577 mD (average 0.084 mD, median 0.059 mD). For Shan 1, corrected porosity ranges from 4.0% to 12.9% (average 6.4%, median 6.0%); corrected permeability from 0.031 to 0.481 mD (average 0.071 mD, median 0.066 mD) (**Table 6**). Per DZ/T 0217-2020, Shanxi Formation sandstones in the Yanchuan East block are overall ultra-low porosity and tight reservoirs (**Table 7**).

Table 7. Reservoir porosity and permeability classification (per Specifications for Calculation of Oil and Gas Reserves, DZ/T 0217-2020).

Classification	Porosity (%)		Permeability (mD)
	Clastic rock porosity (%)	Non-clastic matrix porosity (%)	Reservoir air permeability
Ultra-High	≥30	≥15	≥500
High	≥25 - <30	≥10 - <15	≥100 - <500
Medium	≥15 - <25	≥5 - <10	≥10 - <100
Low	≥10 - <15	≥2 - <5	≥1.0 - <10
Ultra-Low	<10	<2	≥0.1 - <1.0
Tight			<0.1

6. Conclusion

Shanxi Formation reservoirs in the Yanchuan East area are dominated by fine- to medium-grained sandstones, primarily lithic sandstones, lithic quartz sandstones, and quartz sandstones, with detrital components chiefly quartz and metamorphic lithics, and cementation mainly siliceous and carbonate types. Under combined compaction and cementation, reservoirs exhibit ultra-low porosity and tight characteristics overall. Pore types are dominated by volcanic lithic dissolution and residual intergranular pores, with minor intercrystalline pores and microfractures, wherein dissolution and microfractures significantly enhance reservoir quality. Throat structures feature small sizes, poor sorting, and limited connectivity; Shan 2 reservoirs are generally tighter with inferior storage capacity compared to Shan 1, where local high-quality storage spaces develop. Overall, Shanxi Formation reservoirs display pronounced heterogeneity, classified as ultra-low porosity and low-permeability types, but locally developed dissolution pores and fractures provide favorable conduits for natural gas migration and enrichment. Thus, areas of intense dissolution and fracture development should be prioritized as key targets for natural gas exploration and development.

Conflicts of Interest

The authors declare no conflicts of interest regarding the publication of this paper.

References

Abdulhadi, D., Ali, J. A., & Hama, S. M. (2025). Advanced Techniques for Improving the Production of Natural Resources from Unconventional Reservoirs: A State-Of-The-Art Review. *Energy & Fuels, 39,* 10853-10876. https://doi.org/10.1021/acs.energyfuels.5c01259

Ashraf, U., Zhang, H., Anees, A., Mangi, H. N., Ali, M., Zhang, X. et al. (2021). A Core Logging, Machine Learning and Geostatistical Modeling Interactive Approach for Subsurface Imaging of Lenticular Geobodies in a Clastic Depositional System, SE Pakistan. *Natural Resources Research, 30,* 2807-2830. https://doi.org/10.1007/s11053-021-09849-x

Avseth, P., Mukerji, T., Mavko, G., & Dvorkin, J. (2010). Rock-physics Diagnostics of Depositional Texture, Diagenetic Alterations, and Reservoir Heterogeneity in High-Porosity Siliciclastic Sediments and Rocks—A Review of Selected Models and Suggested Work Flows. *Geophysics, 75,* 75A31-75A47. https://doi.org/10.1190/1.3483770

Cui, H., Zhu, S., Gao, Y., & Chen, W. (2025). Hydrothermal Activity near the Permian-Triassic Transition in the South-western Ordos Basin, China: Evidence from Carbonate Cementation in Upper Permian Sandstones. *Sedimentology, 72,* 227-257. https://doi.org/10.1111/sed.13232

Cui, H., Zhu, S., Wang, J., Gao, Y., Wan, C., & Tong, H. (2022). Physical Properties, Pore-Throat Structure, Fractal Characteristics and Their Effects on the Gas-Bearing Capacity of Tight Sandstone: A Case Study from the Northern Tianhuan Depression, Ordos Basin, China. *Natural Resources Research, 31,* 1559-1584. https://doi.org/10.1007/s11053-022-10059-2

Dang, W., Qian, M., Nie, H., Liu, J., Du, K., Feng, Y. et al. (2025). Oil Storage Capacity in Organic-Rich Chang 7 Shale, Ordos Basin: Comparing Evaluation Methods and Controlling Factors. *Geological Journal, 60,* 2176-2194. https://doi.org/10.1002/gj.5167

Fan, C., Nie, S., Li, H., Pan, Q., Shi, X., Qin, S. et al. (2024). Geological Characteristics and Major Factors Controlling the High Yield of Tight Oil in the Da'anzhai Member of the Western Gongshanmiao in the Central Sichuan Basin, China. *Geomechanics and Geophysics for Geo-Energy and Geo-Resources, 10,* Article No. 67. https://doi.org/10.1007/s40948-024-00783-9

Fu, S., Fang, Q., Li, A., Li, Z., Han, J., Dang, X. et al. (2021). Accurate Characterization of Full Pore Size Distribution of Tight Sandstones by Low-Temperature Nitrogen Gas Adsorption and High-Pressure Mercury Intrusion Combination Method. *Energy Science & Engineering, 9,* 80-100. https://doi.org/10.1002/ese3.817

Gao, X., Wang, Y., Li, Y., Guo, H., Ni, X., Wu, X. et al. (2019). Characteristics of Tight Sandstone Reservoirs and Controls of Reservoir Quality: A Case Study of He 8 Sandstones in the Linxing Area, Eastern Ordos Basin, China. *Acta Geologica Sinica—English Edition, 93,* 637-659. https://doi.org/10.1111/1755-6724.13862

Li, J., Gao, C., Zhao, B., & Cheng, X. (2024). Permeability Upscaling Conversion Based on Reservoir Classification. *Processes, 12,* Article 1653. https://doi.org/10.3390/pr12081653

Li, J., Li, X., Tian, W., Xiao, C., Zhao, Y., Xiang, J. et al. (2023). Characterization of the Sedimentary Environment of the Shanxi Formation in the Southeastern Ordos Basin Revealed by Detrital Zircon and Geochemical Analyses. *Minerals, 13,* Article 1331. https://doi.org/10.3390/min13101331

Li, J., Liu, Y., Gao, Y., Cheng, B., Meng, F., & Xu, H. (2018). Effects of Microscopic Pore Structure Heterogeneity on the Distribution and Morphology of Remaining Oil. *Petroleum Exploration and Development, 45,* 1112-1122. https://doi.org/10.1016/s1876-3804(18)30114-9

Li, X., Yang, Z., Li, S., Huang, W., Zhan, J., & Lin, W. (2021a). Reservoir Characteristics and Effective Development Technology in Typical Low-Permeability to Ultralow-Permeability Reservoirs of China National Petroleum Corporation. *Energy Exploration & Exploitation, 39,* 1713-1726. https://doi.org/10.1177/01445987211005212

Li, Y., Fan, A., Yang, R., Sun, Y., & Lenhardt, N. (2021b). Sedimentary Facies Control on Sandstone Reservoir Properties: A Case Study from the Permian Shanxi Formation in the Southern Ordos Basin, Central China. *Marine and Petroleum Geology, 129,* Article ID: 105083. https://doi.org/10.1016/j.marpetgeo.2021.105083

Liu, S., Li, J., Jin, F., Liu, H., Wang, M., Cheng, Y. et al. (2024). Genesis of Efficient Reservoirs in Mixed Sedimentary Setting: A Case Study of Benxi Formation in the Gaoqiao Area, Ordos Basin. *Turkish Journal of Earth Sciences, 33,* 118-145. https://doi.org/10.55730/1300-0985.1903

Lv, D., Zhao, Y., Steel, R. J., Jia, H., Raji, M., Zhang, Z. et al. (2025). Massive Organic Carbon Burial in the North China Basin Is a Main Contributor to Peak Late Paleozoic Ice Age in Early Asselian. *Earth and Planetary Science Letters, 661,* Article ID: 119370. https://doi.org/10.1016/j.epsl.2025.119370

Peng, Z., Qu, J., Chen, C., Wang, H., Zhu, D., Mi, Z. et al. (2025). Coal Accumulation in Marine to Continental Transitional Sequence during Late Carboniferous—Early Permian in the Southeastern Ordos Basin, China. *Geological Journal.* https://doi.org/10.1002/gj.5247

Poda, S., & Talal, G. (2025). Geomechanical and Geochemical Considerations for Hydrogen Storage in Shale and Tight Reservoirs. *Processes, 13,* Article 2522. https://doi.org/10.3390/pr13082522

Ritts, B. D., Weislogel, A., Graham, S. A., & Darby, B. J. (2009). Mesozoic Tectonics and Sedimentation of the Giant Polyphase Nonmarine Intraplate Ordos Basin, Western

North China Block. *International Geology Review, 51,* 95-115. https://doi.org/10.1080/00206810802614523

Shan, X., Guo, H., He, W., Chen, X., Si, X., & Xu, Y. (2021). Impact of Diagenesis on the Sandstone Reservoir Quality: A Case Study from the Lower Jurassic Sangonghe Formation, Junggar Basin, China. *Arabian Journal of Geosciences, 14,* Article No. 2022. https://doi.org/10.1007/s12517-021-08330-6

Tang, T., Li, H., Fu, L., Chen, S., & Wang, J. (2025a). Gas-Water Distribution and Controlling Factors in a Tight Sandstone Gas Reservoir: A Case Study of Southern Yulin, Ordos Basin, China. *Processes, 13,* Article 812. https://doi.org/10.3390/pr13030812

Tang, Y., Jiang, W., Tan, X., Luo, L., Garzanti, E., Gluyas, J. et al. (2025b). Diagenetic Processes Controlled by Volcanic Detritus of the Lower-Middle Permian Shanxi and Shihezi Sandstone Formations, North Ordos Basin, China. *The Depositional Record.* https://doi.org/10.1002/dep2.70030

Tian, X., Bai, Z., Klemperer, S. L., Liang, X., Liu, Z., Wang, X. et al. (2021). *Earth and Planetary Science Letters, 554,* Article ID: 116700. https://doi.org/10.1016/j.epsl.2020.116700

Tong, Q., He, D., Xia, Z., Huang, J., Di, K., Xu, F. et al. (2022). Influence of Reservoir Pore-Throat Structure Heterogeneity on Water-Flooding Seepage: A Case Study of Yanchang Formation in Ordos Basin. *Minerals, 12,* Article 1243. https://doi.org/10.3390/min12101243

Wang, H., Ma, F., Tong, X., Liu, Z., Zhang, X., Wu, Z. et al. (2016). Assessment of Global Unconventional Oil and Gas Resources. *Petroleum Exploration and Development, 43,* 925-940. https://doi.org/10.1016/s1876-3804(16)30111-2

Xiao, L., Yang, L., Zhang, X., Guan, X., & Wei, Q. (2023). Densification Mechanisms and Pore Evolution Analysis of a Tight Reservoir: A Case Study of Shan-1 Member of Upper Paleozoic Shanxi Formation in SW Ordos Basin, China. *Minerals, 13,* Article 960. https://doi.org/10.3390/min13070960

Xu, H., Fan, Y., Hu, F., Li, C., Yu, J., Liu, Z. et al. (2019). Characterization of Pore Throat Size Distribution in Tight Sandstones with Nuclear Magnetic Resonance and High-Pressure Mercury Intrusion. *Energies, 12,* Article 1528. https://doi.org/10.3390/en12081528

Xu, H., Zhou, W., Hu, Q., Yi, T., Ke, J., Zhao, A. et al. (2021a). Quartz Types, Silica Sources and Their Implications for Porosity Evolution and Rock Mechanics in the Paleozoic Longmaxi Formation Shale, Sichuan Basin. *Marine and Petroleum Geology, 128,* Article ID: 105036. https://doi.org/10.1016/j.marpetgeo.2021.105036

Xu, W., Deng, H., & Wang, Y. (2021b). The Sandstone Reservoir Characteristics and Controlling Factors of Shanxi Formation and Lower Shihezi Formation in Southeastern Ordos Basin. *Geological Journal, 56,* 1673-1698. https://doi.org/10.1002/gj.4019

Xue, Y., Dang, W., Zhang, Q., Liu, J., Shangguan, L., Lei, Y. et al. (2024). Lithofacies and Its Reservoir Characteristics of Marine-Continental Transitional Shales: A Case Study of Shanxi Formation in Eastern Ordos Basin. *Energy & Fuels, 38,* 18441-18456. https://doi.org/10.1021/acs.energyfuels.4c02981

Yan, Z., Xiao, W. J., Windley, B. F., Wang, Z. Q., & Li, J. L. (2010). *Sedimentary Geology, 231,* 98-114. https://doi.org/10.1016/j.sedgeo.2010.09.001

Yang, Y., Li, W., & Ma, L. (2005). Tectonic and Stratigraphic Controls of Hydrocarbon Systems in the Ordos Basin: A Multicycle Cratonic Basin in Central China. *AAPG Bulletin, 89,* 255-269. https://doi.org/10.1306/10070404027

Zhang, J., Dang, W., Zhang, Q., Wang, X., Du, G., Shan, C. et al. (2025). Fractal Characterization of Pore Structures in Marine-Continental Transitional Shale Gas Reservoirs: A Case Study of the Shanxi Formation in the Ordos Basin. *Energies, 18,* Article 4013. https://doi.org/10.3390/en18154013

Zhang, W., Shi, Z., & Tian, Y. (2020). An Improved Method to Characterize the Pore-Throat Structures in Tight Sandstone Reservoirs: Combined High-Pressure and Rate-Controlled Mercury Injection Techniques. *Energy Exploration & Exploitation, 38,* 2389-2412. https://doi.org/10.1177/0144598720920729

Zhang, Y., Tian, J., Zhang, X., Li, J., Liang, Q., & Zheng, X. (2022). Diagenesis Evolution and Pore Types in Tight Sandstone of Shanxi Formation Reservoir in Hangjinqi Area, Ordos Basin, Northern China. *Energies, 15,* Article 470. https://doi.org/10.3390/en15020470

Zhong, X., Liu, L., Wang, H., Xu, Z., Chen, H., Wang, X. et al. (2022). Characteristics and Origins of the Modal Pore Throat Structure in Weakly Cemented Sandy Conglomerate Reservoirs. *Journal of Petroleum Science and Engineering, 208,* Article ID: 109470. https://doi.org/10.1016/j.petrol.2021.109470

Zhou, W., Jiao, Y., & Zhao, J. (2017). Sediment Provenance of the Intracontinental Ordos Basin in North China Craton Controlled by Tectonic Evolution of the Basin-Orogen System. *The Journal of Geology, 125,* 701-711. https://doi.org/10.1086/693861

Zou, C. N., Zhang, G. Y., Tao, S. Z., Hu, S. Y., Li, X. D., Li, J. Z. et al. (2010). Geological Features, Major Discoveries and Unconventional Petroleum Geology in the Global Petroleum Exploration. *Petroleum Exploration and Development, 37,* 129-145. https://doi.org/10.1016/s1876-3804(10)60021-3

Zou, C., Zhai, G., Zhang, G., Wang, H., Zhang, G., Li, J. et al. (2015). Formation, Distribution, Potential and Prediction of Global Conventional and Unconventional Hydrocarbon Resources. *Petroleum Exploration and Development, 42,* 14-28. https://doi.org/10.1016/s1876-3804(15)60002-7